Received: 27 February 2018 | Revised: 12 June 2018 | Accepted: 17 June 2018

DOI: 10.1002/aoc.4506

FULL PAPER

WILEY Applied Organometallic Chemistry

p-Toluate-bridged dinuclear Cu(II) complexes in combination with tridentate chelating ligand: Crystal structure, density functional theory calculation, DNA/protein binding and catecholase activity

Samar Dolai[1] | Kalipada Das[1] | Apurba Bhunia[1] | Valerio Bertolasi[2] | Subal Chandra Manna[1]

[1]Department of Chemistry and Chemical Technology, Vidyasagar University, Midnapore 721102, West Bengal, India

[2]Dipartimento di Scienze Chimiche e Farmaceutiche, Centro di Strutturistica Diffrattometrica, Università di Ferrara, Via L. Borsari 46, 44100 Ferrara, Italy

Correspondence
Subal Chandra Manna, Department of Chemistry and Chemical Technology, Vidyasagar University, Midnapore 721102, West Bengal, India.
Email: scmanna@mail.vidyasagar.ac.in

The dinuclear Cu(II) complexes $[Cu_2(L^1)_2(mb)]\cdot ClO_4$ (**1**) and $[Cu_2(L^2)_2(mb)]\cdot ClO_4$ (**2**) (HL^1 = 2-[(2-diethylaminoethylimino)methyl]phenol; HL^2 = 2-[1-(2-diethylaminoethylimino)propyl]phenol; mb = 4-methylbenzoate) were synthesized and characterized using X-ray crystal structure analysis and spectroscopic methods. Complexes **1** and **2** are dinuclear with distorted square pyramidal Cu (II) geometries, where Schiff base coordinates with tridentate (N,N,O) chelating mode and mb bridges two metal centres. Optimized structures and photophysical properties of ligands and complexes were calculated using density functional theory and time-dependent density functional theory methods using B3LYP functional with 6-31G (d,p) and LanL2MB basis sets. Interactions of the complexes with bovine serum albumin (BSA) and human serum albumin (HSA) were studied using UV–visible absorption and fluorescence spectroscopies and the calculated values of association constants (M^{-1}) are 1.7×10^5 (**1**–BSA), 5.7×10^5 (**2**–BSA), 1.6×10^5 (**1**–HSA) and 6.9×10^5 (**2**–HSA). Interactions of the complexes with calf thymus DNA were also investigated and the binding affinities are 1.4×10^5 and 1.6×10^5 M^{-1} for **1** and **2**, respectively. Both complexes catalytically oxidize 3,5-di-*tert*-butylcatechol to 3,5-di-*tert*-butylbenzoquinone in the presence of molecular oxygen.

KEYWORDS
catecholase activity, crystal structure, DFT calculation, dinuclear Cu (II) complex, DNA/protein binding

1 | INTRODUCTION

Transition-metal-based coordination compounds are important due to their potential application in the areas of catalysis,[1] magnetism,[2] medicinal chemistry, etc.[3] Schiff base complexes of 3d metals are important due to their suitable biometric properties that can mimic active site structures of biologically important molecules.[4] Schiff base complexes derived from the condensation of salicylaldehyde and primary amines are studied since these compounds have antiviral, anticancer and antibacterial activities.[5] Copper is a bio-essential element and, due to its biological activity, copper complexes are well studied by inorganic chemists in view of their medicinal applications.[6] Moreover due to the strong Lewis acid property of cupric ion, Cu (II) Schiff base complexes are well studied in the area of DNA cleavage, and recently many Cu(II) complexes of amino acid Schiff base ligands

have shown artificial nuclease activity cleavage.[7,8] Serum albumin is the major soluble protein in the blood and plays an important role for the transportation of many compounds like fatty acids, drugs, pharmaceuticals etc.[9] and the study of the kinetics of interactions of Cu(II) complexes with serum albumins is important for the development of Cu(II) compound-based metallopharmaceuticals. Literature survey reveals that Schiff-base-coordinated Cu(II) complexes are promising candidates for showing catecholase activities.[10]

In the work presented here, we used the Schiff base ligands 2-[(2-diethylaminoethylimino)methyl] phenol (HL^1) and 2-[1-(2-diethylaminoethylimino)propyl] phenol (HL^2) to synthesize the corresponding dinuclear complexes $[Cu_2(L^1)_2(mb)]\cdot ClO_4$ (**1**) and $[Cu_2(L^2)_2(mb)]\cdot ClO_4$ (**2**) (mb = 4-methylbenzoate). In both **1** and **2**, the Schiff bases function as N,N,O donor tridentate chelating/bridging ligands with μ^2-η^2:η^1:η^1 coordination mode (Scheme 1). Electronic absorption spectral properties of complexes and ligands were explained using time-dependent density functional theory (TD-DFT) computation. Using electronic absorption/fluorescence spectroscopic technique, catecholase activities and calf thymus DNA (CT-DNA)/serum albumin interactions of the complexes were studied.

2 | EXPERIMENTAL

2.1 | Materials and Methods

High-purity *N*,*N*-diethylethylenediammine, 2-hydroxypropiophenone, CT-DNA, bovine serum albumin (BSA), human serum albumin (HSA) and ethidium bromide (EtBr) were purchased from Aldrich Chemical Co. All other chemicals were of analytical grade. Solvents used for spectroscopic studies were purified and dried using standard procedures before use.[11]

Elemental analyses (carbon, hydrogen and nitrogen) were performed using a PerkinElmer 240C elemental analyser. Infrared (IR) spectra were recorded with a Bruker Vector 22 FT-IR spectrophotometer operating from 400 to 4000 cm^{-1}. ^1H NMR and ^{13}C NMR spectra of ligands were recorded with a Bruker 400 MHz instrument in $CDCl_3$. Electronic absorption spectra were obtained with a Shimadzu UV-1601 UV–visible spectrophotometer at room temperature. Quartz cuvettes with a 1 cm path length and a 3 cm^3 volume were used for all measurements. Emission spectra were recorded with a Hitachi F-7000 spectrofluorimeter. Room temperature (300 K) spectra were obtained in methanol solution using a quartz cell of 1 cm path length. The slit width was 2.5 nm for both excitation and emission.

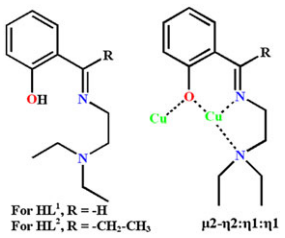

SCHEME 1 Structure of ligands and their coordination mode in complexes

The fluorescence quantum yield was determined using phenol as a reference and water (refractive index η= 1.333) medium for phenol. The solvent used for the complexes was methanol (η= 1.329). Emission spectra were recorded by exciting the complex and the reference phenol at the same wavelength, maintaining nearly equal absorbance (*ca* 0.1). The area of the emission spectrum was integrated using the software available with the instrument and the quantum yield was calculated according to the following equation:

$$\Phi_s = \Phi_r \frac{A_s}{A_r}\frac{I_r}{I_s}\frac{\eta_s^2}{\eta_r^2}$$

where Φ_s and Φ_r are the fluorescence quantum yields of sample and reference, respectively, A_s and A_r are the respective optical densities at the wavelength of excitation, I_s and I_r correspond to the areas under the fluorescence curve and η_s and η_r are the refractive index values for sample and reference, respectively.

2.2 | Synthesis of HL^1 and HL^2

The ligand HL^1 was prepared by condensation reaction of *N*,*N*-diethylethylenediammine and 2-hydroxybenzaldehyde in methanol at 70 °C. A methanolic solution (10 ml) of *N*,*N*-diethylethylenediammine (1 mmol, 0.116 g) was added dropwise to a methanolic solution (10 ml) of 2-hydroxybenzaldehyde (1 mmol, 0.122 g) with constant stirring. The resulting yellow reaction mixture was refluxed (70 °C) for 1 h. The yellow-coloured compound was separated out on evaporation of solvents and the compound was recrystallized using a 1:1 mixture of MeOH and EtOH solvents. Anal. Calcd for $C_{13}H_{20}N_2O$ (220.31) (%): C, 70.87; H, 9.15; N, 12.72. Found (%): C, 70.85; H, 9.12; N, 12.70. ^1H NMR ($CDCl_3$, 200 MHz, δ, ppm): 1.01–1.03 (6H, m, — CH3), 2.35–2.43 (4H, m, — CH_2—), 2.71–2.74 (2H, m, — CH_2— N), 3.60–3.70 (2H, m, — CH_2— N), 4.86 (1H, s, Ar— OH), 6.83–7.41 (4H, m, Ar— H), 8.46 (H, s, — CH= N—). ^{13}C NMR (400 MHz, $CDCl_3$, δ, ppm): 165.84 (— CH= N—), 158.12 (Ar— C— OH), 116.96–132.12 (Ar— C), 44.6–56.90 (N— CH_2— CH_2— N), 14.1 (— CH_3).

The ligand HL^2 was prepared by adopting the same procedure as for HL^1 using 1-(2-hydroxyphenyl)propan-1-one (1 mmol, 0.150 g) instead of 2-hydroxybenzaldehyde. Anal. Calcd for $C_{15}H_{24}N_2O$ (248.36) (%): C, 72.54; H, 9.74; N, 11.28. Found (%): C, 72.52; H, 9.71; N, 11.26. ^{1}H NMR ($CDCl_3$, 200 MHz, δ, ppm): 0.86–0.87 (3H, m, — CH_3), 1.05–1.06 (6H, m, — CH_3), 1.32–1.37 (2H, s, — CH_2—), 2.35–2.43 (4H, m, — CH_2—), 2.73–2.75 (2H, m, — CH_2— N), 3.60–3.70 (2H, m, — CH_2— N), 4.86 (1H, s, Ar— OH), 6.83–7.41 (4H, m, Ar— H). ^{13}C NMR (400 MHz, $CDCl_3$, δ, ppm): 163.84 (— CH═ N—), 156.12 (Ar— C— OH), 116.96–132.12 (Ar— C), 44.6–56.90 (N— CH_2— CH_2— N), 25.6 (aldehyde— CH_2—), 14.1 (amine— CH_3), 7.6 (aldehyde— CH_3).

2.3 | Synthesis of Complexes

Caution! Metal perchlorates in the presence of organic ligands are potentially explosive. Only a small amount of compound should be prepared and it should be handled with care.

The complexes were synthesized by adopting the procedures shown schematically in Scheme 2.

2.3.1 | Synthesis of 1

A methanolic solution (10 ml) of copper perchlorate hexahydrate (1 mmol, 0.370 g) was added dropwise to 15 ml of a methanolic solution of a 1:1 mixture of triethylamine (1 mmol, 0.10 g) and HL^1 (1 mmol, 0.220 g) and stirred for 30 min. To this green-coloured reaction mixture was added an aqueous solution (5 ml) of sodium 4-methylbenzoate (Na (mb); 1 mmol) and the resulting deep-green-coloured reaction mixture stirred for 2 h and filtered. After a few days needle-shaped green crystals suitable for X-ray structure determination were obtained from the filtrate. Yield: 0.268 g (66%).

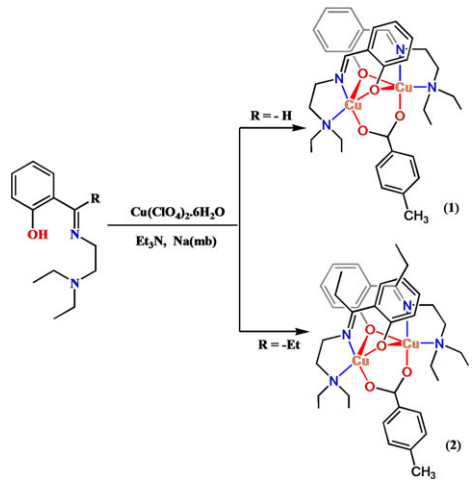

SCHEME 2 Synthesis of **1** and **2**

Anal. Calcd for $C_{34}H_{45}Cu_2N_4O_8Cl$ (800.29) (%): C, 51.03; H, 5.66; N, 7.00. Found (%): C, 51.05; H, 5.63; N, 7.05. IR (KBr, selected bands, cm^{-1}): 2970 (aromatic C— H stretching); 2925 (C (sp^3)— H stretching); 1739 (aromatic $\nu_{C=C}$); 1614 (OCO asymmetric stretching); 1472 (OCO symmetric stretching); 1217 (aromatic $\nu_{C=N}$); 1028 ($\nu_{(ClO4-)}$ asymmetric stretching); 628 ($\nu_{(ClO4-)}$ asymmetric bending).

2.3.2 | Synthesis of 2

Complex **2** was synthesized following the same procedure as adopted for **1** using HL^2 (1 mmol, 0.248 g) instead of HL^1. Green blocked-shaped single crystals of suitable

TABLE 1 Crystal data and details of structure refinement for complexes **1** and **2**

	1	2
Empirical formula	$C_{34}H_{45}Cu_2N_4O_8Cl$	$C_{38}H_{53}Cu_2N_4O_8Cl$
Formula mass	800.27	856.37
Crystal system	Monoclinic	Orthorhombic
Space group	P21	Pccn
a (Å)	8.0267(2)	8.4410(2)
b (Å)	21.3991(6)	13.8710(4)
c (Å)	10.6538(3)	34.2848 (10)
α (°)	90	90
β (°)	98.8210 (17)	90
γ (°)	90	90
Z	2	4
T (K)	295	295
V (Å^3)	1808.30(9)	4014.24 (19)
D_{calcd} (g cm^{-3})	1.470	1.417
μ(mm^{-1})	1.305	1.180
F(000)	832	1792
θrange (°)	2.7–30.1	3.4–27.5
No. of collected data	19146	26343
No. of unique data	9565	4575
R_{int}	0.044	0.055
h,k,l_{max}	11,30,14	10,18,44
Observed [$I > 2\sigma(I)$]	7808	3419
Goodness of fit (F^2)	1.087	1.015
Parameters refined	447	243
$R1[I > 2\sigma(I)]^a$	0.0452	0.0648
$wR2[I > 2\sigma(I)]^a$	0.1179	0.2041
$\Delta\rho$ (e Å^{-3})	−0.54, 0.50	−0.63, 0.64

[a] $R1\ (F_o) = \Sigma||F_o|-|F_c||/\Sigma|F_o|$, $wR2\ (F_o^2) = [\Sigma w\ (F_o^2 - F_c^2)^2/\Sigma w\ (F_o^2)^2]^{1/2}$.

X-ray diffraction quality were obtained after a few days on keeping the filtrate at room temperature. Yield: 0.269 g (63%). Anal. Calcd for $C_{38}H_{53}Cu_2N_4O_8Cl$ (856.37) (%): C, 53.29; H, 6.23; N, 6.54. Found (%): C, 53.25; H, 6.21; N, 6.51. IR (KBr, selected bands, cm^{-1}): 2973 (aromatic C— H stretching); 2938 (C (sp^3)— H stretching); 1739 (aromatic $\nu_{C=C}$); 1589 (OCO asymmetric stretching); 1412 (OCO symmetric stretching); 1321 (aromatic $\nu_{C=N}$); 1079 ($\nu_{(ClO4-)}$ asymmetric stretching); 621 ($\nu_{(ClO4-)}$ asymmetric bending).

2.4 | Crystallographic Data Collection and Refinement

The crystal data of complexes **1** and **2** were collected at room temperature (295 K) using a Nonius Kappa CCD diffractometer with graphite monochromated Mo-K α radiation. The data sets were integrated with the Denzo-SMN package[12] and corrected for Lorentz, polarization and absorption effects (SORTAV).[13] The structures were solved by direct methods using the SIR97[14] system of programs and refined using full-matrix least-squares with all non-hydrogen atoms anisotropically and hydrogens included on calculated positions, riding on their carrier atoms. Both the complex cation and ClO_4^- anion of complex **2** are situated on a two-fold axis passing through the C16, C17, C20 and C21 atoms of the mb ligand and the Cl atom of the perchlorate anion. The atomic groups $C9H_2$, $C12H_2$-$C13H_3$ and $C14H_2$-$C15H_3$ of complex **2** were found disordered and refined over two sites with occupancies of 0.6 and 0.4, respectively. All calculations were performed using SHELXL-97[15] and PARST[16] implemented in the WINGX[17] system of programs. Details of crystallographic data collection and refinement are given in Table 1.

2.5 | Theory and Computational Methods

Theoretical calculations for complexes and ligands were carried out using Gaussian 09 (G09) software,[18] using Becke's three-parameter hybrid exchange functional and

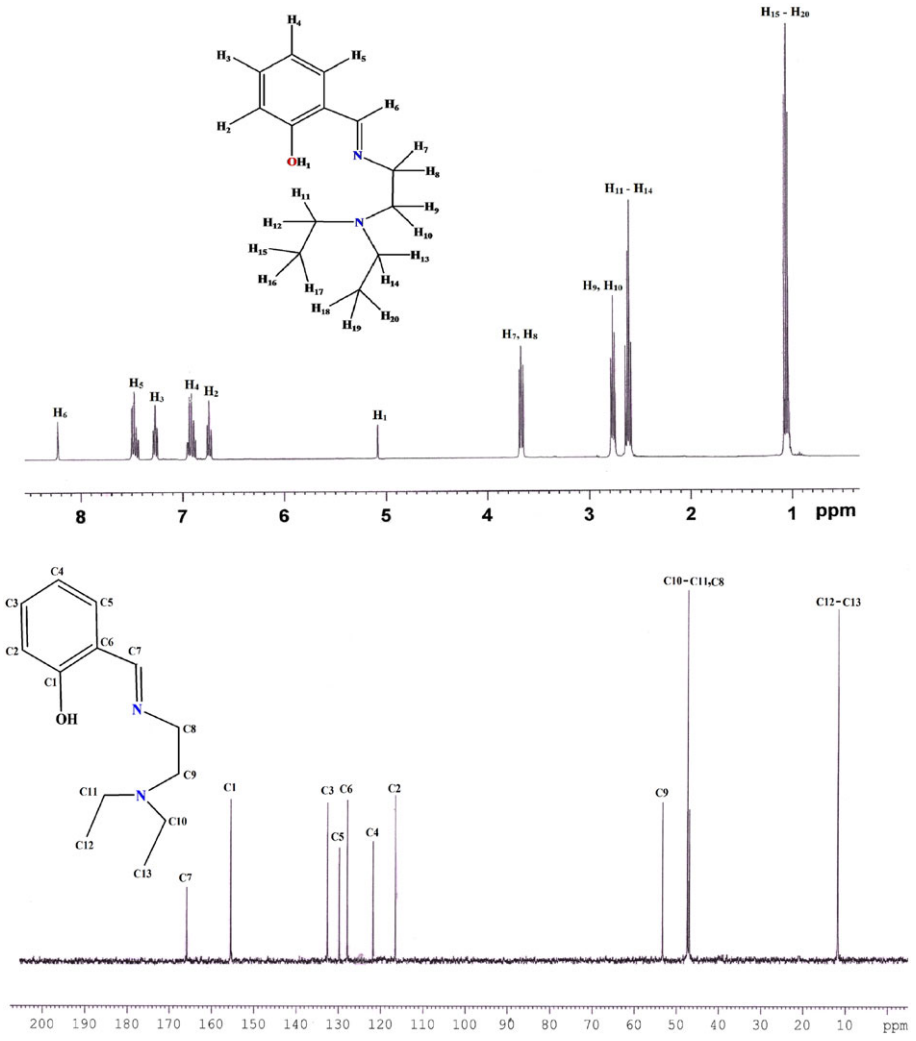

FIGURE 1 ^1H NMR and ^{13}C NMR spectra of HL^1 (in $CDCl_3$)

the Lee–Yang–Parr non-local correlation (B3LYP) functional. The Los Alamos effective core potentials plus MBS (LanL2MB)[19] (for **1** and **2**) and 6-31G (d, p) (for HL^1 and HL^2) basis sets were used for calculation. In this study the ligands were optimized in the ground state (singlet) and structures of the complexes were fully optimized in the ground state (triplet) at the B3LYP level and vibrational frequency calculations were performed to ensure that the optimized geometries represent local minima associated with positive eigen values only.

TD-DFT calculations were performed (in the gas phase for **1** and **2**, and using the conductor-like polarizable continuum model (CPCM) in MeOH for HL^1 and HL^2) to obtain possible vertical electronic excitations.[20] For the calculation of fractional contribution of various group to each molecular orbital, GaussSum[21] was used.

2.6 | Albumin Binding Studies

Interactions of complexes with serum albumins were investigated using the fluorescence spectroscopic technique. Stock solutions of HSA (4.24 μM) and BSA (3.13 μM) were prepared in HEPES buffer (pH = 7.2) and solutions of **1** and **2** (0.1665 μM) were prepared in water. The quenching of fluorescence intensity of serum albumin upon addition of complexes is mainly due to association of serum albumin with complex, serum albumin denaturation or conformational change of serum albumin.[22]

2.7 | DNA Binding Studies

2.7.1 | Electronic absorption spectral studies

UV–visible absorption spectral titration is a useful technique for distinguishing different binding modes of complexes with CT-DNA. Hypochromism or hyperchromism with red or blue shift is often observed in the absorption spectrum of a metal complex when it is bound to DNA. Generally intercalative binding mode between CT-DNA and a complex results in hypochromism and bathochromism (red shift) in the UV–visible absorption spectrum, whereas hyperchromism in the absorption spectrum indicates electrostatic or non-intercalative binding mode. For both complexes **1** and **2** UV–visible absorption spectral titrations were performed at a fixed concentration of complexes (2 ml, 13.04 μM) with gradual addition of 2 μl of 90.9 μM CT-DNA solution. Intrinsic binding constants (K_{ib}) of the complexes with CT-DNA were determined using the equation[23]

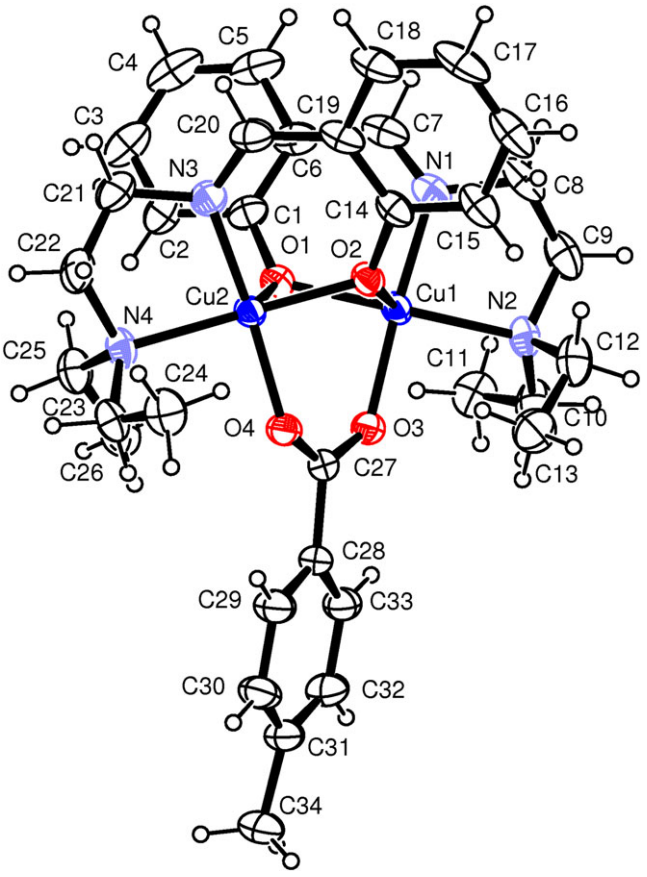

FIGURE 2 ORTEP view of cationic unit of complex **1** showing thermal ellipsoids at 30% probability level

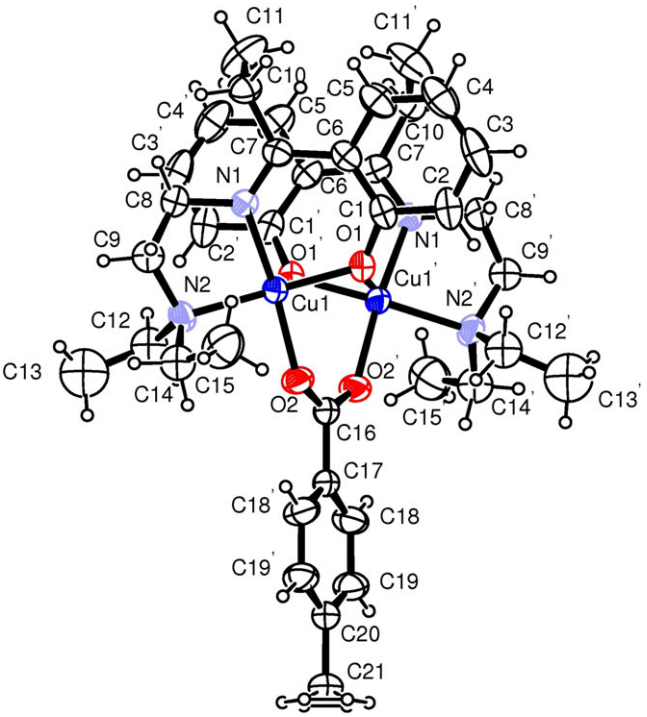

FIGURE 3 ORTEP view of cationic unit of complex **2** showing thermal ellipsoids at 30% probability level

$$\frac{[DNA]}{\varepsilon_a - \varepsilon_f} = \frac{[DNA]}{\varepsilon_b - \varepsilon_f} + \frac{1}{K_{ib}(\varepsilon_b - \varepsilon_f)}$$

where [DNA] is the concentration of CT-DNA, ε_a is the extinction coefficient of the complex at a given CT-DNA concentration and ε_f and ε_b are the extinction coefficients of the complex in free solution and when fully bound to CT-DNA, respectively. A plot of [DNA]/($\varepsilon_a - \varepsilon_f$) versus [DNA] gives a straight line with $1/(\varepsilon_b - \varepsilon_f)$ and $1/K_{ib}$ ($\varepsilon_b - \varepsilon_f$) as slope and intercept, respectively.

2.7.2 | Competitive binding fluorescence measurement

The competitive binding nature of the complexes with CT-DNA was investigated by adopting the fluorescence spectroscopic method using aqueous solution of EtBr-bound CT-DNA in HEPES buffer (pH = 7.2). EtBr shows fluorescence and the intensity of such fluorescence increases approximately 20-fold in the presence of CT-DNA. The increase in fluorescence intensity is due to intercalation of the planar EtBr phenanthridium ring between nearby base pairs of the CT-DNA double helix. Fluorescence spectral titrations were carried out with gradual addition of 2 μl of 13.04 μM solution of complexes to a solution of EtBr-bound CT-DNA (2 ml, 90.9 μM aqueous solution). The fluorescence intensity at 607 nm (λ_{ex} = 500 nm) gradually decreased keeping emission wavelength fixed. The Stern–Volmer equation[24] ($I_0/I = 1 + K_{sv}$ [quencher], where I_0 and I are the emission intensity in the absence and presence of complex, K_{sv} is the Stern–Volmer constant and [quencher] is the concentration of Cu (II) complex) was used to calculate the quenching constant (K_{sv}).

3 | RESULTS AND DISCUSSION

3.1 | Synthetic Aspects

Multidentate coordinating ligands HL^1 and HL^2 were prepared by a one-pot synthesis employing condensation of corresponding amine and aldehyde in methanol under reflux condition. They were characterized using NMR

TABLE 2 Experimental and calculated[a] coordination bond distances (Å) and angles (°) for complexes **1** and **2**

Bond length			Bond angle		
	Exp	Calcd		Exp	Calcd
Complex **1**					
Cu(1)–O(1)	1.928(2)	2.037	O(1)–Cu(1)–O(2)	85.57(9)	75.00
Cu(1)–O(2)	2.449(2)	2.398	O(1)–Cu(1)–N(1)	92.71 (13)	91.00
Cu(1)–O(3)	1.938(2)	1.929	O(1)–Cu(1)–N(2)	163.82 (12)	163.72
Cu(1)–N(1)	1.936(4)	1.974	O(1)–Cu(1)–O(3)	89.87 (10)	92.52
Cu(1)–N(2)	2.080(3)	2.300	O(2)–Cu(1)–O(3)	94.62(9)	90.14
Cu(2)–O(1)	2.455(2)	2.228	O(2)–Cu(1)–N(1)	92.30 (11)	101.96
Cu(2)–O(2)	1.938(2)	2.043	O(2)–Cu(1)–N(2)	110.46 (10)	120.81
Cu(2)–O(4)	1.938(2)	1.939	O(3)–Cu(1)–N(1)	172.78 (13)	167.87
Cu(2)–N(3)	1.927(3)	1.974	N(1)–Cu(1)–N(2)	84.70 (14)	82.24
Cu(2)–N(4)	2.106(3)	2.284	O(1)–Cu(2)–O(2)	85.16(9)	77.47
Cu(1) ... Cu(2)	3.108(6)	3.317	O(4)–Cu(2)–N(3)	173.12 (12)	170.64
			τ_5 parameter	0.0056	0.0461
Complex **2**					
Cu(1)–O(1)	1.888(3)	2.008	O(1)–Cu(1)–O(2)	91.3(1)	89.23
Cu(1)–O(1′)	2.592(3)	2.213	O(1)–Cu(1)–N(2)	166.8(1)	150.81
Cu(1)–O(2)	1.956(3)	2.279	O(1)–Cu(1)–O(1′)	82.6(1)	75.34
Cu(1)–N(1)	1.944(3)	2.026	O(1′)–Cu(1)–O(2)	90.9(1)	88.76
Cu(1)–N(2)	2.070(3)	2.185	O(1′)–Cu(1)–N(1)	93.2(1)	89.45
Cu(1) ... Cu (1′)	3.249(7)	3.235	O(2)–Cu(1)–N(1)	173.7(1)	131.78
			τ_5 parameter[26]	0.115	0.317

[a]Complexes optimized in gas phase; LanL2MB basis set; B3LYP functional.

spectroscopy (Figure 1 and Figures 1S and 2S). Using HL^1 or HL^2 in combination with mb, complexes **1** and **2** were synthesized.

3.2 | Crystal structures of 1 and 2

ORTEP views[25] of the cationic units of complexes **1** and **2** are shown in Figures 2 and 3, respectively. Both **1** and **2** consist of two metal centres, namely Cu1 and Cu2, which are crystallographically independent but chemically similar. The geometries around Cu (II) atoms are distorted square pyramidal, and the equatorial plane of which is occupied by one oxygen atom and two nitrogen atoms of respective N,N,O donor Schiff base ligands, while the fourth coordination site is occupied by the oxygen atom of mb. Selected bond distances and angles are listed in Table 2.

Complex **1** crystallizes in the monoclinic crystal system of P21 space group, while complex **2** crystallizes

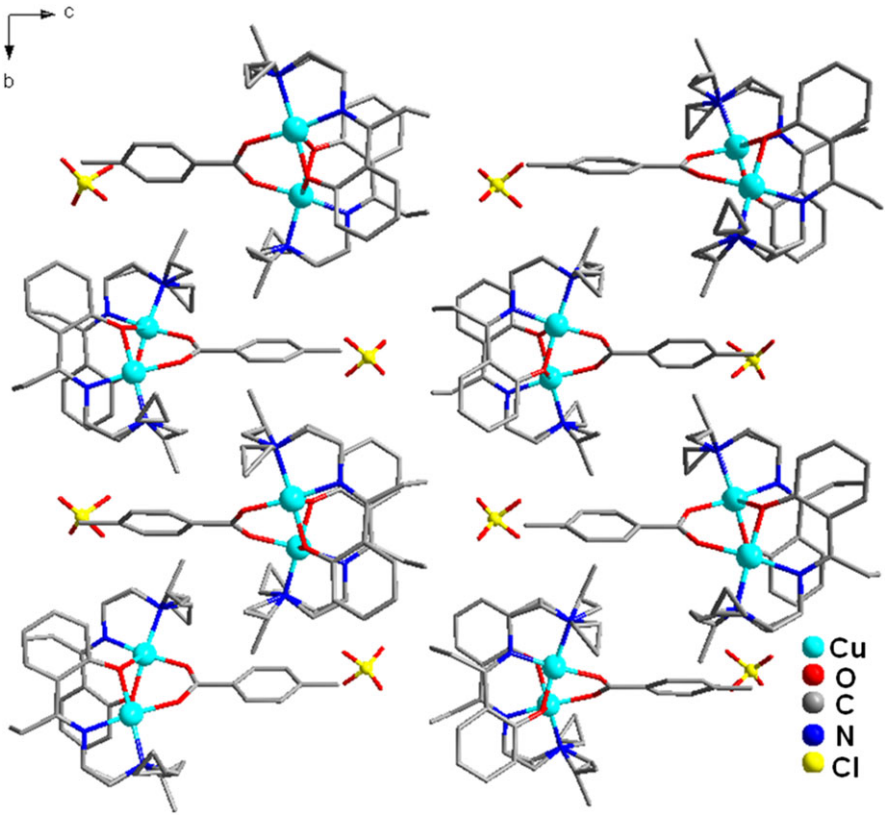

FIGURE 4 Packing diagram of complex **2**

TABLE 3 Selected UV–visible energy transitions at the TD-DFT[a]/B3LYP level for ligands and complexes

	Excited state	λ_{cal} (nm), ε_{cal} (M^{-1} cm^{-1}), (eV)	Oscillator strength (f)	λ_{exp} (nm), ε_{exp} (M^{-1} cm^{-1}), (eV)	Key transition	Character[b]
HL^1	S_8	278.9, (10668.42), 4.44	0.0804	278, (0.030×10^5), 4.45	HOMO-1 → LUMO (30%)	π → π*
HL^2	S_{19}	213.06, (16650.91), 5.81	0.2095	213, (0.129×10^5), 5.82	HOMO-3 → LUMO (10%) HOMO-1 → LUMO+1 (17%)	π → π* π → π*
	S_8	276.13, (9457.38), 4.49	0.1288	276, (0.018×10^5), 4.45	HOMO-1 → LUMO (39%)	π → π*
1	T_{27}	372.19, (26867.32), 3.33	0.0080	370, (0.130×10^6), 3.34	HOMO (β) → LUMO+2 (β) (21%)	ILCT
2	T_{26}	369.92, (27032.66), 3.35	0.0046	369, (2.71×10^7), 3.36	HOMO-1 (β) → LUMO+2 (β) (17%)	IELCT

[a]For HL^1 and HL^2: using CPCM in methanol; basis set, 6-31G (d-p). For complexes **1** and **2**: in gas phase; basis set, LanL2MB.

[b]ILCT, intra-ligand charge transfer from L to L; IELCT, inter-ligand charge transfer from mb to L.

in orthorhombic crystals of space group Pccn. In both complexes, the bond lengths between Cu atom and nitrogen atoms are within the range 1.936(4) to 2.106(3) Å (Table 2). The average bond angle around the Cu centre is *ca* 90°, whereas the lowest bond angle is observed for N(1)–Cu(1)–N(2) at 84.70 (14)°. The Schiff base ligand is coordinated in a tridentate fashion to the metal centre (Cu1) through one phenoxy oxygen (O1/O2) and two nitrogen (N1 and N2) atoms, and forms an equatorial plane with one carboxylate oxygen (O3/O4).

In both complexes, the equatorial Cu-O bond length (1.928(2) Å for **1**, 1.888(3) Å for **2**) is shorter than the axial Cu-O bond length (2.455(2) Å for **1**, 2.592(3) for **2**) due to Jahn–Teller distortion. The Cu-O bond lengths vary from 1.928(2) to 2.455(2) Å for **1** and 1.888(3) to 2.592(3) Å for **2**. The Cu-N bond lengths vary from 1.927 to 2.106 Å for **1** and 1.944 to 2.070 Å for **2** (Table 2). The distance between the two copper atoms in **1** is 3.108 Å, and in **2** is 3.249 Å, indicating that there is no bond between the two metal centres. Crystal packing of **1** and **2** is shown in Figures 3S and 4, respectively.

Calculated values of the trigonality parameter[26] τ are 0.0056 and 0.115 for **1** and **2**, respectively, indicating that both the complexes possess distorted square pyramidal geometry.

3.3 | Photophysical Study of Ligands

The electronic absorption spectrum of HL^1 shows major transitions at 215 nm ($\varepsilon \sim 0.179 \times 10^5\ M^{-1}\ cm^{-1}$), 254 nm ($\varepsilon \sim 0.087 \times 10^5\ M^{-1}\ cm^{-1}$), 278 nm ($\varepsilon \sim 0.030 \times 10^5\ M^{-1}\ cm^{-1}$), 316 nm ($\varepsilon \sim 0.039 \times 10^5\ M^{-1}\ cm^{-1}$) and 400 nm ($\varepsilon \sim 0.012 \times 10^5\ M^{-1}\ cm^{-1}$). The spectrum of HL^2 shows significant transitions at 213 nm ($\varepsilon \sim$

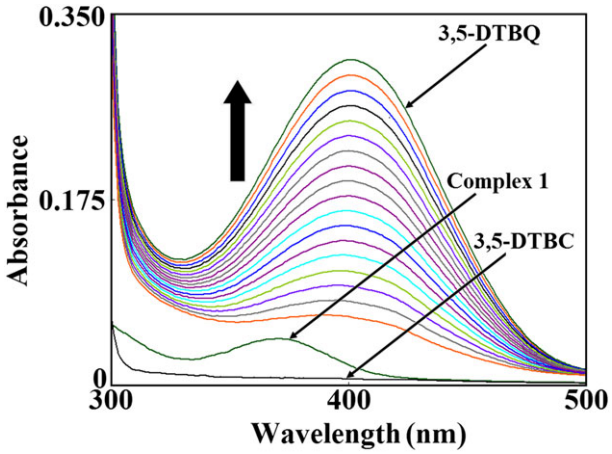

FIGURE 6 Increase in 3,5-DTBQ band at 400 nm after addition of 10^{-4} M methanolic solution of complex **1** to 100-fold methanolic solution of 3,5-DTBC. The spectra were recorded at intervals of 5 min

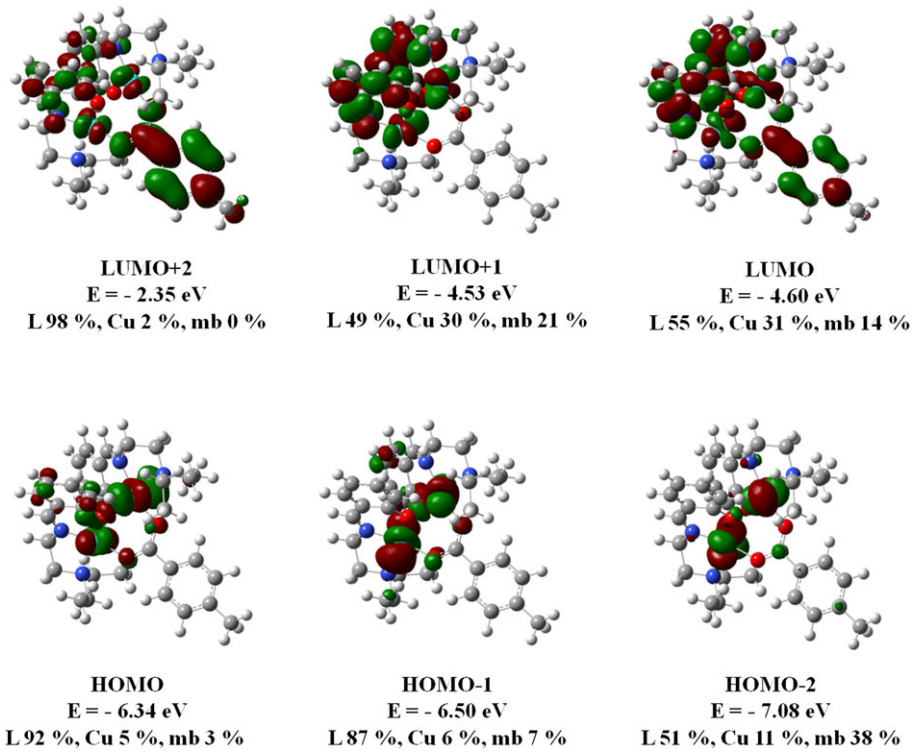

FIGURE 5 Surface plots of frontier orbitals (β-MOs) along with their energies and compositions of **1** using B3LYP functional in gas phase (basis set: LanL2MB)

0.129×10^5 M^{-1} cm^{-1}), 250 nm ($\varepsilon \sim 0.060 \times 10^5$ M^{-1} cm^{-1}), 276 nm ($\varepsilon \sim 0.018 \times 10^5$ M^{-1} cm^{-1}), 323 nm ($\varepsilon \sim 0.023 \times 10^5$ M^{-1} cm^{-1}) and 390 nm ($\varepsilon \sim 0.012 \times 10^5$ M^{-1} cm^{-1}). The absorption bands appearing at around 200 nm to 400 nm are due to n → π*/π → π* (Table 3).

3.4 | IR, Electronic Absorption and Fluorescence Spectra of Complexes

The most important IR spectral bands of **1** and **2** are summarized in Section 2 and tabulated in Table 1S. Aromatic ν(C═ C, C═ N) stretching vibrations of complexes appear in the region 1217–1739 cm^{-1}, and the bands in the region 2970–2973 cm^{-1} correspond to aromatic ν(C— H) stretching vibrations. Aliphatic ν(C (sp^3)— H) stretching vibration appear at 2925 and 2938 cm^{-1} for **1** and **2**, respectively (Figures 4S and 5S). The ν_{as} (OCO) stretching vibrations for **1** and **2** appear at 1614 and 1589 cm^{-1}, respectively. Whereas ν_s (OCO) stretching vibrations appear at 1472 and 1412 cm^{-1} for **1** and **2**, respectively. The separation of stretching frequencies $\Delta\nu(= \nu_{as}\text{ (OCO)} - \nu_s\text{ (OCO)})$ for **1** and **2** are 142 and 177 cm^{-1}, respectively. But for divalent metal carboxylates the observed trend is $\Delta\nu_{(chelating)} < \Delta\nu_{(bridging)} < \Delta\nu_{(ionic)} < \Delta\nu_{(monodentate)}$.[27] It is noted that Δν for Na_2 (mb) is 227 cm^{-1}. Therefore Δνfor the complexes is less than Δ νfor Na_2 (mb), and the observed moderate Δ νvalues of the complexes (142 and 177 cm^{-1}) corroborate the crystallographically observed bridging of carboxylate group in **1** and **2**.

Electronic spectra of both complexes were recorded in methanol solution. The spectrum of **1** shows four strong transitions at 202 nm ($\varepsilon \sim 1.21 \times 10^6$ M^{-1} cm^{-1}), 222 nm

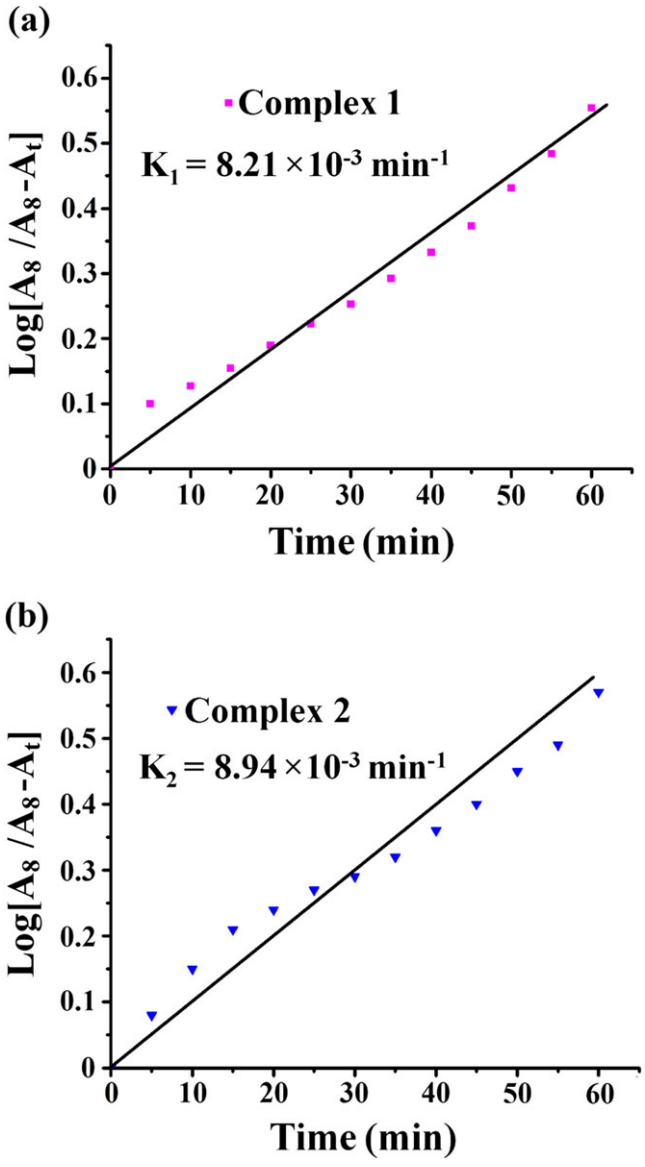

FIGURE 7 Change in absorption maxima at 400 nm with time after addition of 10^{-4} M methanolic solution of complex to 100-fold methanolic solution of 3,5-DTBC: (a) complex **1**; (b) complex **2**

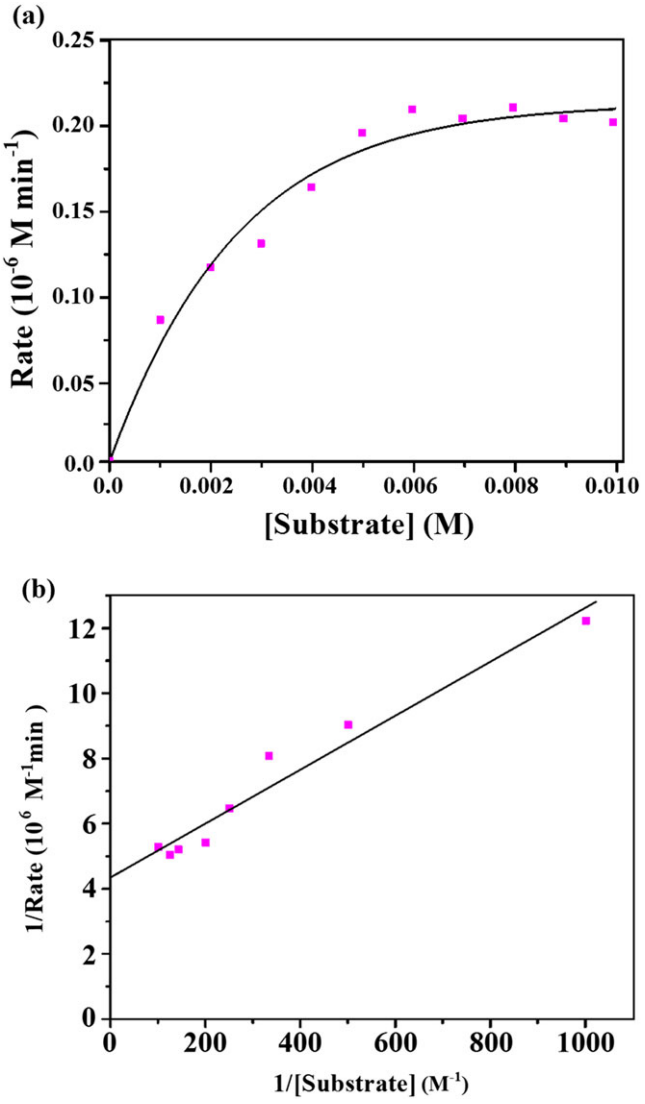

FIGURE 8 (a) Rate versus substrate concentration and (b) Lineweaver–Burk plot for complex **1**

($\varepsilon \sim 0.97 \times 10^6\ M^{-1}\ cm^{-1}$), 271 nm ($\varepsilon \sim 0.51 \times 10^6\ M^{-1}\ cm^{-1}$) and 370 nm ($\varepsilon \sim 0.13 \times 10^6\ M^{-1}\ cm^{-1}$) (Figure 6S). For **2**, the transitions appear at 202 nm ($\varepsilon \sim 1.04 \times 10^6\ M^{-1}\ cm^{-1}$), 225 nm ($\varepsilon \sim 0.64 \times 10^6\ M^{-1}\ cm^{-1}$), 269 nm ($\varepsilon \sim 0.3 \times 10^6\ M^{-1}\ cm^{-1}$) and 369 nm ($\varepsilon \sim 0.09 \times 10^6\ M^{-1}\ cm^{-1}$) (Figure 7S).

When excited at 271 nm (λ_{ex}), a methanolic solution of **1** shows fluorescence emission at 306 nm (λ_{em}) with quantum yield of 0.35. On the other hand, when excited at 269 nm (λ_{ex}), **2** also shows emission at the same wavelength of 306 nm (λ_{em}) with quantum yield of 0.41 (Table 2S).

3.5 | DFT and TD-DFT Computations

3.5.1 | DFT and TD-DFT computations of HL^1 and HL^2

DFT and TD-DFT calculation of HL^1 and HL^2 were performed with B3LYP functional using 6-31G (d, p) basis set. Optimized structures of ligands are shown in Figures 8S and 9S, and physical parameters and energies of molecular orbitals are presented in Table 3S. TD-DFT calculations were performed in methanol using CPCM and theoretically possible spin-allowed (singlet–singlet) electronic transitions with their assignment are presented in Table 3 and Tables 4S and 5S. For both HL^1 and HL^2, HOMO → LUMO is the lowest energy transition, whereas HOMO −2 → LUMO +1 and HOMO −1 → LUMO +1 transitions are the possible highest energy transitions in HL^1 and HL^2, respectively. For HL^1, the experimental electronic spectral (Figure 10S) band at 276 nm may be assigned as HOMO −1 → LUMO transition (Table 3). On the other hand for HL^2 the spectral (Figure 10S) bands at 213 and 278 nm may be assigned as (HOMO −1 → LUMO; HOMO −3 → LUMO +1) and HOMO −1 → LUMO transitions, respectively. The spectral bands at 213, 276 and 278 nm correspond to $\pi \rightarrow \pi^*$ transition.

3.5.2 | DFT and TD-DFT computations of complexes

Optimized structures of **1** and **2** along with their Mulliken charge distributions are shown in Figures 11S and 12S. Calculated energies of optimized geometries and other physical parameters are presented in Table 7S. For **1**, the α-state HOMO and LUMO energies are −6.57 and − 2.39 eV, respectively, and the β-state HOMO and LUMO energies are −6.34 and − 4.60 eV, respectively. Whereas for **2**, the α-state HOMO and LUMO energies are −5.01 and − 2.04 eV, respectively, and the β-state HOMO and LUMO energies are −5.55 and − 3.86 eV, respectively. Surface plots of frontier molecular orbitals of **1** and **2** are shown in Figures 5 and 13S.

The contributions of Schiff base (L^1/L^2), copper and carboxylate (mb) to the HOMO (α) of complexes are 95% L^1, 3% Cu, 2% mb (for **1**) and 76% L^2, 24% Cu, 0% mb (for **2**), and for LUMO (α) the corresponding values are 98% L^1, 2% Cu, 0% mb (for **1**) and 4% L^2, 2% Cu, 94% mb (for **2**). The contributions of Schiff base (L^1/L^2), copper and carboxylate (mb) to the HOMO (β) of complexes are 92% L^1, 5% Cu, 3% mb (for **1**) and 92% L^2, 8% Cu, 0% mb (for **2**), and for LUMO (β) the values are 55% L^1, 31% Cu, 14% mb (for **1**) and 68% L^2, 32% Cu, 0% mb (for **2**). From the DFT/TD-DFT calculations, the values of electronic spectral transition wavelength (λ_{cal}) and oscillator strength (f) were determined, and are presented in Tables 9S and 10S. The experimentally observed

TABLE 4 Kinetic parameters for oxidation of 3,5-DTBC catalysed by complexes **1** and **2** and reported dinuclear Cu (II) complexes in methanol solvent

Complex	V_{max}	K_M (M)	K_{cat} (h^{-1})	K_{cat}/K_M ($M^{-1}\ h^{-1}$)	Ref.
$[Cu_2\ (L^1)_2(mb)]\cdot ClO_4$ (**1**)	$(2.31 \pm 0.31) \times 10^{-7}$	$(1.90 \pm 0.23) \times 10^{-3}$	42 ± 0.09	$(22.07 \pm 0.41) \times 10^3$	This work
$[Cu_2\ (L^2)_2(mb)]\cdot ClO_4$ (**2**)	$(2.91 \pm 0.38) \times 10^{-7}$	$(2.76 \pm 0.35) \times 10^{-3}$	52.9 ± 0.12	$(19.11 \pm 0.32) \times 10^3$	This work
$[Cu_2\ (L^3)(OMe)][ClO_4]_2\cdot 2MeOH$		$(2.3 \pm 0.2) \times 10^{-3}$	33		[28a]
$[Cu_2\ (L^4)(OMe)(MeOH)(ClO_4)]ClO_4$		$(3.1 \pm 0.2) \times 10^{-4}$	48		[28a]
$[Cu_2\ (L^5)(OMe)(MeOH)(ClO_4)]ClO_4$		$(1.4 \pm 0.2) \times 10^{-3}$	43		[28a]
$[Cu_2L^6\ (ClO_4)_2]$		$(3.32 \pm 0.06) \times 10^{-3}$	93.6	28.2×10^3	[10a]
$[Cu_2L^6\ (OH)]ClO_4$		$(4.60 \pm 0.2) \times 10^{-3}$	233.4	50.7×10^3	[10a]
$[Cu_2\ (H_2L^7)(\mu\text{-}OH)](ClO_4)_2$			28.74		[28b]
$[Cu_2\ (L^{H,H}\text{-}O^8)(OH)(MeCN)_2][ClO_4]_2$			55		[28c]

HL^3, 4-bromo-2-(4-methylpiperazin-1-ylmethyl)-6-[(2-pyridylmethyl)aminomethyl]phenol; HL^4, 4-bromo-2-(4-methylpiperazin-1-ylmethyl)-6-{[2-(2-pyridyl)ethyl]aminomethyl}phenol; HL^5, 4-bromo-2-(4-methylpiperazin-1-ylmethyl)-6-{[2-(1-methyl-2-imidazolyl)ethyl]aminomethyl}phenol; HL^6, 2-[[2-(diethylamino)ethylamino]methyl]phenol; H_3L^7, 2,6-bis[{[(2-hydroxybenzyl)(*N*′,*N*′-(dimethylamino)ethyl)}amino}methyl]-4-methylphenol; $L^{H,H}\text{-}O^8$, 1,3-bis[(*N*,*N*-dimethylaminoethyl)aminomethyl]benzene.

spectral transitions (Figures 14S and 15S) at 370 nm (for **1**) and 369 nm (for **2**) are due to HOMO (β) → LUMO +2 (β) (21%) and HOMO −1(β) → LUMO +2 (β) (17%) transitions, respectively. For **1**, compositions of HOMO (β) and LUMO +2(β) molecular orbitals are (92% L^1, 5% Cu, 3% mb) and (98% L^1, 2% Cu, 0% mb), respectively. For **2**, compositions of HOMO −1 (β) and LUMO +2 (β) molecular orbitals are (63% L^2, 36% Cu, 1% mb) and (7% L^2, 2% Cu, 91% mb), respectively. Therefore electronic spectral band at 370 nm for **1** is due to intra-ligand charge transfer in L, and that at 369 nm for **2** is due to inter-ligand charge transfer from mb to L.

3.6 | Catechol Oxidation Studies of Complexes

Catecholase activities of complexes **1** and **2** were examined at room temperature (30 °C) by adding their 1×10^{-4} M methanolic solution to a 1×10^{-2} M methanolic solution of 3,5-di-*tert*-butylcatechol (3,5-DTBC) in the presence of molecular oxygen, and the progress of the reaction was studied by recording UV absorption spectra of the mixture at five-minute intervals. The changes of the electronic absorption spectra of 3,5-DTBC in the presence of the complexes are shown in Figures 6 and 16S.

A band at 400 nm corresponding to 3,5-di-*tert*-butylquinone (3,5-DTBQ) gradually increases with time after addition of complexes. The kinetics of oxidation of 3,5-DTBC to 3,5-DTBQ were determined by monitoring the growth of the 400 nm band as function of time (t). From the $\log[(A_\infty - A_0)/(A_\infty - A_t)]$ (where A_∞ and A_t are the absorbance at infinite time and at t, respectively) versus t plots (Figure 7), the rate constants for complex–substrate mixtures were determined and the calculated values were 8.21×10^{-3} and 8.94×10^{-3} min^{-1} for **1** and **2**, respectively.

To determine the dependence of reaction rate on substrate concentration, we added solutions of complex to 3,5-DTBC solutions of various concentrations (1×10^{-3} to 10×10^{-3} M) and observed a first-order dependence of reaction rate at low concentration of substrate, and saturation kinetics at higher concentration of 3,5-DTBC (Figures 8 and 17S).

As the complexes show saturation kinetics, we used the Michaelis–Menten model for these systems. Using the Lineweaver–Burk equation, $1/V = (K_M/V_{max})(1/[S]) + 1/V_{max}$, the kinetic parameters V_{max}, K_M and K_{cat} were determined (Table 4) from a plot of $1/V$ versus $1/[S]$. Complex **2** shows higher turnover number (K_{cat}/K_M) than complex **1**, indicating higher catalytic activity (Table 4). The observed catalytic rate can be explained considering the deviation from ideal geometry. Calculated τ values indicate more deviation from regular geometry observed for **2** than **1**, which corroborate the observed order of catalytic activity. Kinetic parameters of catecholase activities of reported dinuclear Cu (II) complexes[10a, 28] are presented in Table 4 and these results indicate that **1** and **2** have catalytic activities comparable to those of reported compounds.

3.7 | Protein Binding Studies

3.7.1 | Electronic absorption spectral titration

Electronic absorption spectra were recorded in the range 200–500 nm using various concentrations of the Cu (II) complexes with a constant concentration of BSA and HSA. Electronic spectra of both BSA and HSA show an

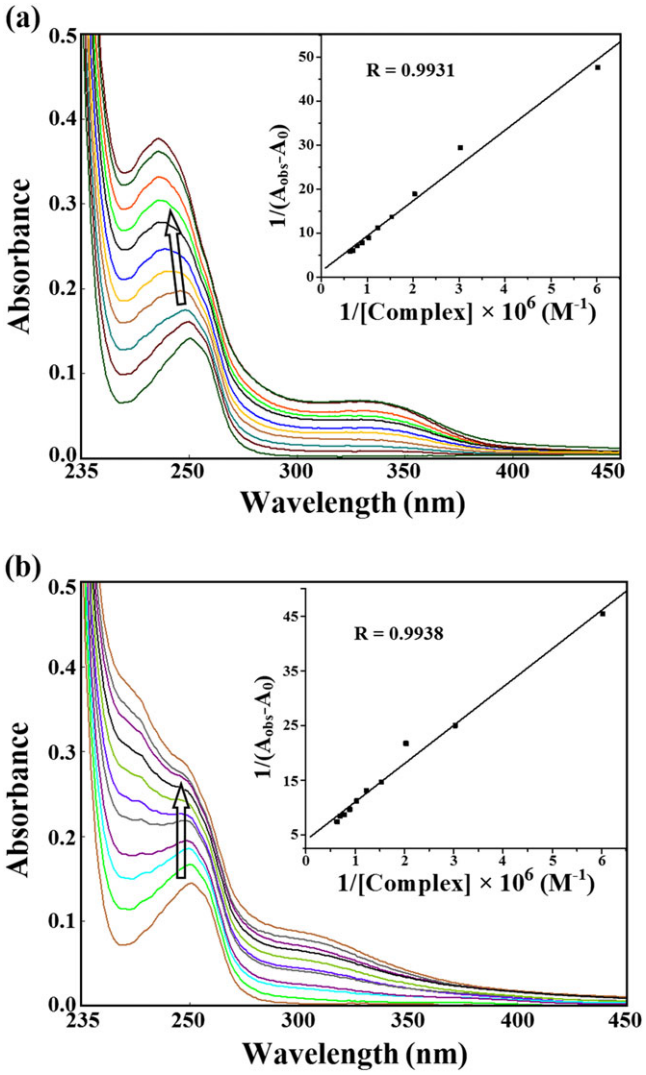

FIGURE 9 Change of UV–visible absorption spectra of BSA (2 ml, 3.13 μM aqueous solution) upon gradual addition of 10 μl of 0.1665 μM aqueous solution of (a) complex **1** and (b) complex **2**. Insets: $1/(A_{obs} - A_0)$ versus 1/[complex] plots of BSA absorption titration

absorption band at 280 nm. Gradual addition of 10 μl of 0.1665 μM aqueous solution of the complexes to 2 ml of 3.13 μM BSA solution results in an increase in absorbance with blue shift for both complexes (280 to 265 nm for **1**, 280 to 272 nm for **2**) (Figure 9).

Similarly electronic absorption spectra of HSA also show a blue shift with increase in absorbance (280 to 258 nm for **1**, 280 to 272 nm for **2**) (Figure 18S) upon gradual addition of 10 μl of 0.1665 μM aqueous solution of the complexes to 2 ml of 4.24 μM solution of HSA. This hypsochromic shift of the spectral band corresponds to ground-state association between complex and serum albumin. The apparent association constants (K_{app}) were calculated using the following equation:[29]

$$\frac{1}{A_{obs}-A_0} = \frac{1}{A_c-A_0} + \frac{1}{K_{app}(A_c-A_0)[complex]}$$

where A_{obs} is the observed absorbance at 280 nm of the solution containing various concentrations of the complex, A_0 is the absorbance of serum albumin only and A_c is the absorbance of serum albumin with complex. A plot of $1/(A_{obs} - A_0)$ versus 1/[complex] results in a straight line (Figure 9 insets) with slope of $1/K_{app}$ $(A_c - A_0)$. From this slope the values of K_{app} were calculated, and the calculated values are 1.7×10^5 M^{-1} (for **1**) and 5.7×10^5 M^{-1} (for **2**) for BSA, and 1.6×10^5 M^{-1} (for **1**) and 6.9×10^5 M^{-1} (for **2**) for HSA (Table 5). These results indicate that the strength of interaction varies in the order **1** <**2**.

3.7.2 | Fluorometric protein binding studies

To solutions of serum albumins (4.24 μM HSA; 3.13 μM BSA) in HEPES buffer (pH = 7.2), Cu (II) complexes were added at room temperature, and the quenching of emission intensities at 340 nm (λ_{ex} = 280 nm) for BSA (Figure 10) and 330 nm (λ_{ex} = 280 nm) for HSA (Figure 19S) was recorded after gradual addition of 10 μl of 0.1665 μM aqueous solutions of **1** and **2**.

Upon gradual increasing of complex concentration, the fluorescence intensities of BSA and HSA were significantly decreased. Moreover the electronic absorption spectra of the serum albumins show significant change in the presence of the complexes. These observations clearly indicate that the fluorescence quenching occurs through a ground-state association process. The Stern–Volmer equation[24] $(I_0/I = 1 + K_{sv}[quencher] = 1 + k_q\tau_0[quencher]$, where I_0 and I are the emission intensity in the absence and presence of complex, K_{sv} is the Stern–Volmer constant, [quencher] is the concentration of Cu (II) complex, k_q is the quenching constant and τ_0 is the lifetime (*ca* 10^{-8} s) of the fluorophore in absence of quencher) was used to estimate the observed fluorescence quenching behaviour, and the calculated values of K_{sv} are 4.4×10^5 M^{-1} (for **1**–BSA) and 5.2×10^5 M^{-1} (for **2**–BSA) (Figure 20S). The calculated values of k_q are 4.4×10^{13} M^{-1} s^{-1} (**1**–BSA) and 5.2×10^{13} M^{-1} s^{-1} (**2**–BSA). For HSA, the calculated values of K_{sv} are 4.8×10^5 M^{-1} (for **1**–HSA) and 4.9×10^5 M^{-1} (for **2**–HSA) (Figure 21S), and k_q are 4.8×10^{13} M^{-1} s^{-1} (**1**–HSA) and 4.9×10^{13} M^{-1} s^{-1}

TABLE 5 Kinetic parameters of interaction of BSA/HSA with **1** and **2** and reported Cu (II) complexes

Compound	K_{app} (M^{-1})	n	K_b (M^{-1})	K_{sv} (M^{-1})	k_q (M^{-1} s^{-1})	Ref
BSA						
$[Cu_2 (L^1)_2(mb)]\cdot ClO_4$ (**1**)	1.7×10^5	0.70	4.7×10^5	4.4×10^5	4.4×10^{13}	This work
$[Cu_2 (L^2)_2(mb)]\cdot ClO_4$ (**2**)	5.7×10^5	0.76	5.8×10^5	5.2×10^5	5.2×10^{13}	This work
$[Cu_2 (L^9)_2(N_3)_2]$		1.06	2.92×10^5	8.24×10^4	5.15×10^{12}	[30]
$[Cu_2 (L^{10})$ Cl $(CH_3OH)(dabt)]\cdot CH_3OH$			8.35×10^4	8.70×10^4	8.70×10^{12}	[31]
$[Cu_2 (L^{10})(bpy)(H_2O)](pic)\cdot H_2O$				1.18×10^5	1.18×10^{13}	[31]
HSA						
$[Cu_2 (L^1)_2(mb)]\cdot ClO_4$ (**1**)	1.6×10^5	0.70	4.9×10^5	4.8×10^5	4.8×10^{13}	This work
$[Cu_2 (L^2)_2(mb)]\cdot ClO_4$ (**2**)	6.9×10^5	1.02	5.7×10^5	4.9×10^5	4.9×10^{13}	This work
$[Cu_2 (L^9)_2(N_3)_2]$		1.39	1.28×10^5	7.57×10^4	4.73×10^{12}	[30]
$[Cu (L^{11})(OAc)]\cdot H2O$		0.70	0.14×10^5		7.3×10^{12}	[32]
$[Cu (HL^{11})(C_2O_4)$ (EtOH)]·EtOH		1.15	1.67×10^5		5.3×10^{12}	[32]
$[Cu (L^{11})(bza)]$		1.11	1.52×10^5		6.6×10^{12}	[32]
$[Cu (L^{11})(sal)]$		1.18	3.38×10^5		6.8×10^{12}	[32]

HL^9, ligand derived from 2-acetylpyridine and thiosemicarbazide; HL^{10}, *N*-phenolato-*N*′-[2-(dimethylamino)ethyl]oxamide; HL^{11}, 1-(((2-((2-hydroxypropyl) amino)ethyl)imino)methyl)naphthalene-2-ol.

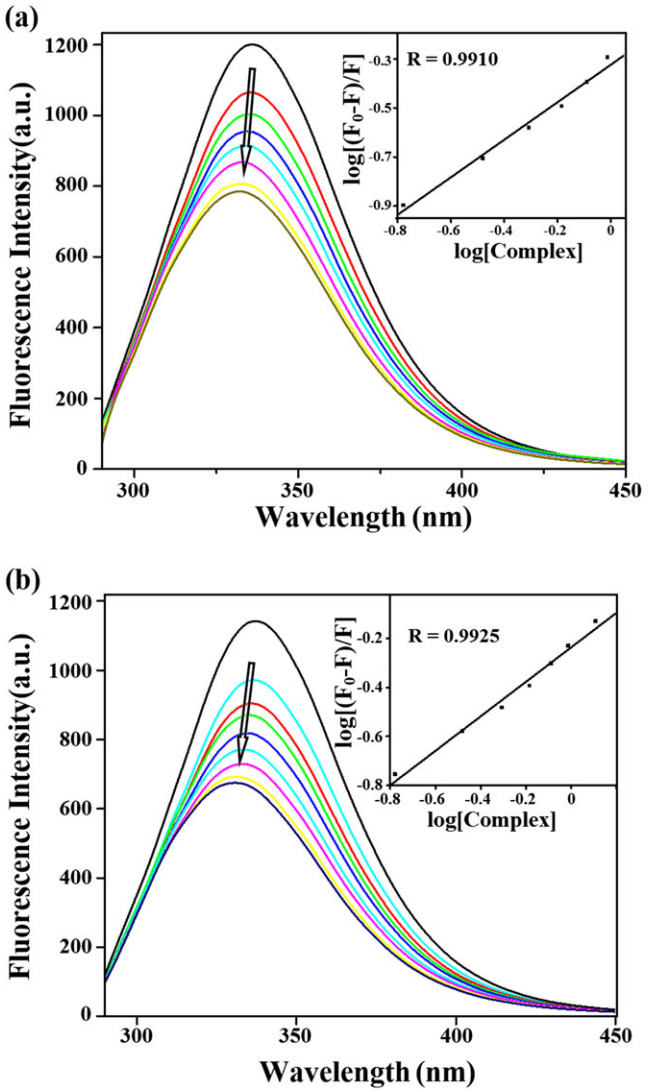

FIGURE 10 Change of fluorescence spectra of BSA (2 ml, 3.13 μM) upon gradual addition of 10 μl of 0.1665 μM aqueous solution of (a) complex **1** and (b) complex **2**. Insets: Scatchard plots of the BSA fluorescence titration

(**2**–HSA). The values of K_{sv} and k_q indicate that complex **2** has a good fluorescence quenching ability in comparison to complex **1**.

The equilibrium between free and protein-bound complexes is expressed by the Scatchard equation:[33]

$$\log\frac{(F_0-F)}{F} = \log k_b + n\log[\text{complex}]$$

where k_b is the binding constant of complex with serum albumin and n is the number of binding sites per serum albumin molecule. A plot of $\log\frac{(F_0-F)}{F}$ versus log [complex] gives a straight line (insets of Figures 10 and 19S) with n and log k_b as slope and intercept, respectively.

The binding constants and the number of binding sites per albumin were calculated and the calculated values are given in Table 5. A comparison of kinetic parameters of BSA/HSA interaction of reported Cu (II) complexes (Table 5) shows that **1** and **2** have relatively strong interaction compared with the reported compounds.[30–32]

3.8 | DNA Binding Studies of Complexes

3.8.1 | Electronic absorption spectral study

Figure 11 shows the change in electronic absorption spectra of complexes with gradual addition (2 μl, 90.9 μM) of CT-DNA solution to solutions of complexes (2 ml, 13.04 μM). The absorbance of the 268 nm band of complex **1** gradually increases with blue shift and finally appears at 265 nm. For **2**, the absorbance of the 266 nm spectral

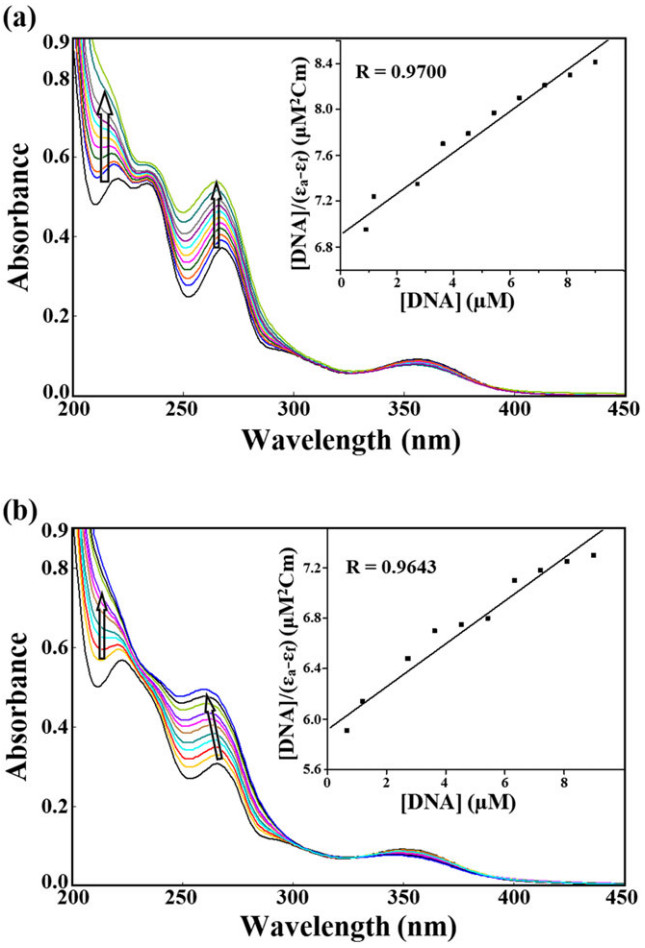

FIGURE 11 Change of electronic absorption spectra of (a) complex **1** and (b) complex **2** (2 ml, 13.04 μM) in HEPES buffer upon gradual addition of 2 μl of 90.9 μM aqueous solution of CT-DNA

TABLE 6 Kinetic parameters of interaction of CT-DNA with complexes **1** and **2** and reported dinuclear Cu (II) complexes

Compound	K_{sv} (M^{-1})	K_{ib} (M^{-1})	Ref.
$[Cu_2(L^1)_2(mb)]\cdot ClO_4$	2.8×10^4	1.4×10^5	This work
$[Cu_2(L^2)_2(mb)]\cdot ClO_4$	2.9×10^4	1.6×10^5	This work
$\{[Cu_2(L^{12})bipy)]\cdot(ClO_4)_2\cdot CH_3CN\}_n$		0.72×10^5	[35]
$\{[Cu_2(L^{13})(bipy)]\cdot(ClO_4)_2\cdot H_2O\}_n$		2.1×10^5	[35]
$[Cu_2(L^{14})_2(H_2O)]_n$		0.049×10^5	[36]
$\{[Cu_2(L^{15})_2(H_2O)]\ H_2O\}_n$		0.008×10^5	[36]

H_2L^{12}, [2 + 2] condensation product of 1,3-diaminopropane with 2,6-diformyl-4-methylphenol; H_2L^{13}, [2 + 2] condensation product of 1,3-diaminopropane with 2,6-diformyl-4-fluorophenol; H_2L^{14}, Schiff base derived from condensation of *N*-(2-hydroxybenzaldehyde) with L-methionine; H_2L^{15}, reduced form of H_2L^8.

band gradually increases with blue shift (up to 6 nm) and finally the band appears at 260 nm.

Hyperchromism (Figure 11) with blue shift of spectral band reveals non-intercalative/electrostatic binding mode of complexes with CT-DNA.[34] The calculated values of binding constant K_{ib} are 1.4×10^5 and 1.6×10^5 M^{-1} for **1** and **2**, respectively (Table 6).

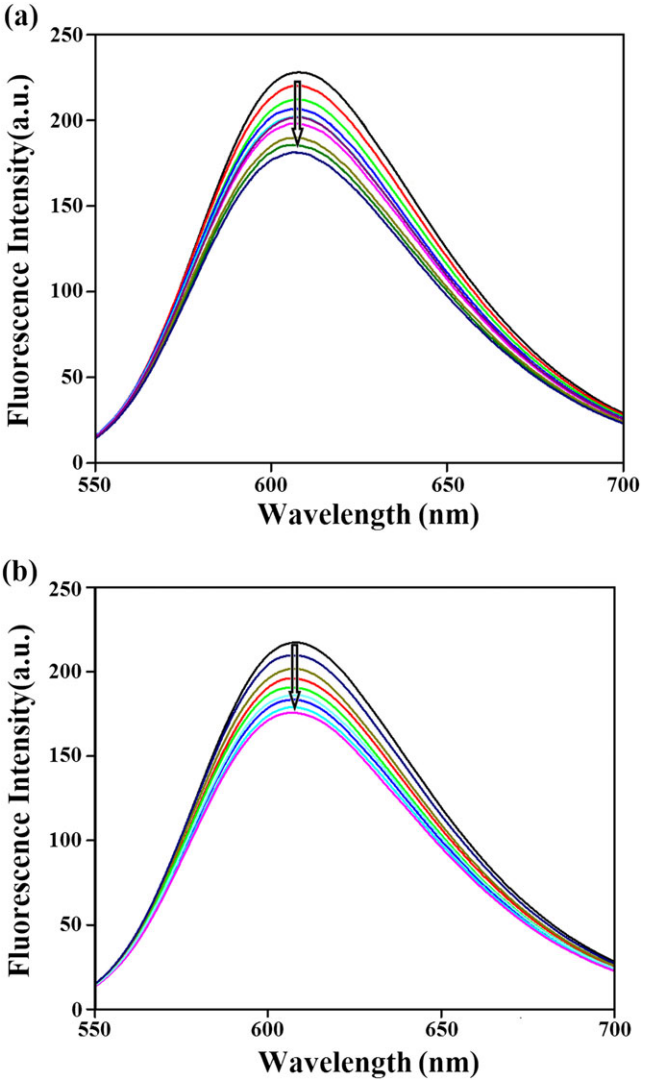

FIGURE 12 Change of fluorescence spectra of EtBr–CT-DNA upon gradual addition of (a) complex **1** and (b) complex **2** (2 μl, 13.043 μM) in HEPES buffer

3.8.2 | EtBr displacement studies

EtBr-bound CT-DNA shows emission at 607 nm on excitation at 500 nm. Figure 12 shows the change of fluorescence spectra of EtBr-bound CT-DNA upon gradual addition of 2 μl of a 13.043 μM solution of complexes.

Fluorescence intensity of EtBr-bound CT-DNA gradually decreases with increasing concentration of complexes. Hypochromism in the presence of the complexes suggests that the complexes displace the EtBr molecules from the DNA binding sites. From the Stern–Volmer plot (Figure 22S) the binding constants (K_{sv}) were calculated and the calculated values are 2.8×10^4 and 2.9×10^4 M^{-1} for **1** and **2**, respectively. Table 6 presents the kinetic parameters of the interaction of CT-DNA with reported dinuclear copper complexes. A comparison of results shows that complexes **1** and **2** have stronger interaction than the reported complexes.[35,36]

4 | CONCLUSIONS

In summary, we have presented here the synthesis, crystal structure, DFT calculation, DNA/protein binding and catecholase activities of two *p*-toluate-bridged isostructural dinuclear Cu (II) complexes. Results of DFT calculations for **1** and **2** are in good agreement with their crystallographically determined structures and the possible spin-allowed triplet–triplet electronic transitions of the complexes and singlet–singlet electronic transitions of ligands have been assigned based on the results obtained from TD-DFT calculations. We have also conducted TD-DFT calculations for the complexes in singlet state and the results are summarized in the supporting information. A comparison of singlet- and triplet-state DFT results reveals that the triplet-state

DFT results are closer to the experimental results. CT-DNA/protein binding of the complexes was investigated using electronic absorption and fluorescence spectroscopic techniques and the results show that both compounds effectively bind with CT-DNA and serum albumins. Complexes **1** and **2** are active for catalysing oxidation of 3,5-DTBC to 3,5-DTBQ in the presence of molecular oxygen in methanol, and the observed rate of oxidation is higher where the complex deviates more from its regular geometry.

ACKNOWLEDGEMENTS

The authors gratefully acknowledge the financial assistance given by the CSIR, Government of India, to S.C.M. (project no. 01 (2743)/13/EMR-II). S.D. is grateful to UGC, India, for providing a fellowship. S.C.M. thanks UGC-SAP, DST-FIST New Delhi USIC (VU) and Vidyasagar University for infrastructural facilities.

ORCID

Subal Chandra Manna http://orcid.org/0000-0001-6823-1209

REFERENCES

[1] a) M. Eddaoudi, H. Li, O. M. Yaghi, *J. Am. Chem. Soc.* **2000**, *122*, 1391; b) R. Tagore, R. H. Crabtree, G. W. Brudvig, *Inorg. Chem.* **2008**, *47*, 1815; c) J. S. Fossey, R. Matsubara, H. Kiyohara, S. Kobayashi, *Inorg. Chem.* **2008**, *47*, 781; d) N. Gharah, S. Chakraborty, A. K. Mukherjee, R. Bhattacharyya, *Chem. Commun.* **2004**, 2630.

[2] a) T. Shiga, K. Maruyama, G. N. Newton, R. Inglis, E. K. Brechin, H. Oshio, *Inorg. Chem.* **2014**, *53*, 4272; b) S. Mistri, E. Zangrando, A. Figuerola, A. Adhikary, S. Konar, J. Cano, S. C. Manna, *Cryst. Growth Des.* **2014**, *14*, 3276; c) P. Seth, A. Figuerola, J. Jover, E. Ruiz, A. Ghosh, *Inorg. Chem.* **2014**, *53*, 9296.

[3] a) B. Duff, V. R. Thangella, B. S. Creaven, M. Walsh, D. A. Egan, *Eur. J. Pharmacol.* **2012**, *689*, 45; b) A. T. Chaviara, P. C. Christidis, A. Papageorgiou, E. Chrysogelou, D. J. Hadjipavlou-Litina, C. A. Bolos, *J. Inorg. Biochem.* **2005**, *99*, 2102; c) L. E. McQuade, S. J. Lippard, *Inorg. Chem.* **2010**, *49*, 7464. d) A. Chakraborty, P. Kumar, K. Ghosh, P. Roy, *Eur. J. Pharmacol.* **2010**, *647*, 1.

[4] J. Adhikary, P. Chakraborty, S. Das, T. Chattopadhyay, A. Bauzá, S. K. Chattopadhyay, B. Ghosh, F. A. Mautner, A. Frontera, D. Das, *Inorg. Chem.* **2013**, *52*, 13442.

[5] a) J.-L. Zeng, S.-B. Yu, Y.-M. Jiang, L.-X. Sun, Z. Cao, D.-W. Yang, *J. Chem. Crystallogr.* **2010**, *40*, 761; b) Y.-M. Jiang, S.-H. Zhang, Q. Xu, Y. Xiao, *Acta Chim. Sin.* **2003**, *61*, 573; c) S.-H. Zhang, Y.-M. Jiang, X.-X. Zhong, *Chin. J. Inorg. Chem.* **2004**, *20*, 959.

[6] a) D. R. Green, J. C. Reed, *Science* **1998**, *281*, 1309; b) Y. Ma, L. Cao, T. Kavabata, T. Yoshino, B. B. Yang, S. Okada, *Free Radic. Biol. Med.* **1998**, *25*, 568; c) F. Liang, C. Wu, H. Lin, T. Li, D. Gao, Z. Li, J. Wei, C. Zheng, M. Sun, *Bioorg. Med. Chem. Lett.* **2003**, *13*, 2469; d) J. Easmon, G. Pürstinger, G. Heinisch, T. Roth, H. H. Fiebig, W. Holzer, W. Jäger, M. Jenny, J. Hofmann, *J. Med. Chem.* **2001**, *44*, 2164.

[7] L. Li, J. Dong, J. Li, B. Jing, D. Wang, *Transition Met. Chem.* **2011**, *36*, 289.

[8] J. Li, J. Dong, H. Cui, T. Xu, L. Li, *Transition Met. Chem.* **2012**, *37*, 175.

[9] a) B. X. Huang, H. Y. Kim, C. Das, *J. Am. Soc. Mass Spectrom.* **2004**, *15*, 1237. b) S. Shi, Y. Zhang, X. Chen, M. Peng, *J. Agric. Food Chem.* **2011**, *59*, 10761.

[10] a) A. Biswas, L. K. Das, M. G. B. Drew, C. Diaz, A. Ghosh, *Inorg. Chem.* **2012**, *51*, 10111; b) S. Mistri, A. Paul, A. Bhunia, R. Manne, M. K. Santra, H. Puschmann, S. C. Manna, *Polyhedron* **2016**, *104*, 63; c) A. Bhunia, S. Manna, S. Mistri, A. Paul, R. K. Manne, M. K. Santra, V. Bertolasi, S. C. Manna, *RSC Adv.* **2015**, *5*, 67727.

[11] D. D. Perrin, W. L. F. Armarego, D. R. Perrin, *Purification of Laboratory Chemicals*, Pergamon Press, Oxford **1980**.

[12] Z. Otwinowski, W. Minor, in *Methods in Enzymology*, (Eds: C. W. Carter, R. M. Sweet) Vol. Part A, Vol. 276, Academic Press, London **1997** 307.

[13] R. H. Blessing, *Acta Crystallogr. A* **1995**, *51*, 33.

[14] A. Altomare, M. C. Burla, M. Camalli, G. L. Cascarano, C. Giacovazzo, A. Guagliardi, A. G. Moliterni, G. Polidori, R. Spagna, *J. Appl. Cryst.* **1999**, *32*, 115.

[15] G. M. Sheldrick, *SHELX-97, program for crystal structure refinement*, University of Gottingen, Germany **1997**.

[16] M. Nardelli, *J. Appl. Cryst.* **1995**, *28*, 659.

[17] L. J. Farrugia, *J. Appl. Cryst.* **1999**, *32*, 837.

[18] Gaussian 09, revision A.02, Gaussian Inc., Wallingford, CT, **2009**.

[19] P. J. Hay, W. R. Wadt, *J. Chem. Phys.* **1985**, *82*, 270.

[20] R. E. Stratmann, G. E. Scuseria, M. J. Frisch, *J. Chem. Phys.* **1998**, *109*, 8218.

[21] N. M. O'Boyle, A. L. Tenderholt, K. M. Langner, *J. Comput. Chem.* **2008**, *29*, 839.

[22] a) A. Basu, D. Thiyagarajan, C. Kar, A. Ramesh, G. Das, *RSC Adv.* **2013**, *3*, 14088; b) P. Krishnamoorthy, P. Sathyadevi, A. H. Cowley, R. R. Butorac, N. Dharmaraj, *Eur. J. Med. Chem.* **2011**, *46*, 3376.

[23] A. Wolfe, G. H. Shimer, T. Mechan, *Biochemistry* **1987**, *22*, 6392.

[24] J. R. Lakowicz, *Principles of Fluorescence Spectroscopy*, 3rd ed., Springer, New York **2006**.

[25] M. N. Burnett, C. K. Johnson, Report ORNL-6895, Oak Ridge National Laboratory, Oak Ridge, TN, **1996**.

[26] A. W. Addison, T. N. Rao, J. Reedijk, J. V. Rijn, G. C. Verschoor, *J. Chem. Soc. Dalton Trans.* **1984**, 1349.

[27] a) K. Nakamoto, *Infrared Spectra of Inorganic and Coordination Compounds*, John Wiley, New York **1997**; b) V. Zelenak, Z. Vargova, K. Gyoryova, *Spectrochim. Acta A* **2007**, *66*, 262; c) G. B. Deacon, R. J. Phillip, *Coord. Chem. Rev.* **1980**, *33*, 227; d) W. Lewandowski, M. Kalinowska, H. Lewandowska,

J. Inorg. Biochem. **2005**, *99*, 1407; e) S. Mistri, E. Zangrando, P. Vojtısek, S. C. Manna, *ChemistrySelect* **2017**, *2*, 2634.

[28] a) J. Reim, B. Krebs, *J. Chem. Soc. Dalton Trans.* **1997**, 3793; b) A. Banerjee, S. Sarkar, D. Chopra, E. Colacio, K. K. Rajak, *Inorg. Chem.* **2008**, *47*, 4023; c) S. Mandal, J. Mukherjee, F. Lloret, R. N. Mukherjee, *Inorg. Chem.* **2012**, *51*, 13148.

[29] a) A. Wolfe, G. H. Shimer, T. Mechan, *Biochemistry* **1987**, *26*, 6392; b) A. Paul, S. Mistri, A. Bhunia, S. Manna, H. Puschmann, S. C. Manna, *RSC Adv.* **2016**, *6*, 60487.

[30] N. Biswas, S. Khanra, A. Sarkar, S. Bhattacharjee, D. P. Mandal, A. Chaudhuri, S. Chakraborty, C. R. Choudhury, *New J. Chem.* **2017**, *41*, 12996.

[31] K. Zheng, F. Liu, X.-M. Xu, Y.-T. Li, Z.-Y. Wua, C.-W. Yan, *New J. Chem.* **2014**, *38*, 2964.

[32] W.-J. Lian, X.-T. Wang, C.-Z. Xie, H. Tian, X.-Q. Song, H.-T. Pan, X. Qiao, J.-Y. Xu, *Dalton Trans.* **2016**, *45*, 9073.

[33] a J. R. Lakowicz, *Principles of Fluorescence Spectroscopy*, Kluwer Academic/Plenum, New York **1999** 53; b X.-Z. Feng, Z. Lin, L.-J. Yang, C. Wang, C.-L. Bai, *Talanta* **1998**, *47*, 1223.

[34] a) F. Mancin, P. Scrimin, P. Tecilla, U. Tonellato, *Chem. Commun.* **2005**, 2540; b) L. Tjioe, A. Meininger, T. Joshi, L. Spiccia, B. Graham, *Inorg. Chem.* **2011**, *50*, 4327.

[35] Q. R. Cheng, F. Q. Zhang, H. Zhou, Z. Q. Pan, G. Y. Liao, *J. Coord. Chem.* **2015**, *68*, 1997.

[36] C. Gao, X. Ma, J. Lu, Z. Wang, J. Tian, S. Yan, *J. Coord. Chem.* **2011**, *64*, 2157.

SUPPORTING INFORMATION

Additional supporting information may be found online in the Supporting Information section at the end of the article.

How to cite this article: Dolai S, Das K, Bhunia A, Bertolasi V, Manna SC. *p*-Toluate-bridged dinuclear Cu(II) complexes in combination with tridentate chelating ligand: Crystal structure, density functional theory calculation, DNA/protein binding and catecholase activity. *Appl Organometal Chem*. 2018;e4506. https://doi.org/10.1002/aoc.4506